Two-dimensional dipolar nematic colloidal crystals

M. Škarabot,[1] M. Ravnik,[2] S. Žumer,[1,2] U. Tkalec,[1] I. Poberaj,[2] D. Babič,[2] N. Osterman,[2] and I. Muševič[1,2]
[1]*J. Stefan Institute, Jamova 39, 1000 Ljubljana, Slovenia*
[2]*Faculty of Mathematics and Physics, University of Ljubljana, Jadranska 19, 1000 Ljubljana, Slovenia*
(Received 21 June 2007; published 27 November 2007)

We study the interactions and directed assembly of dipolar nematic colloidal particles in planar nematic cells using laser tweezers. The binding energies for two stable configurations of a colloidal pair with homeotropic surface alignment are determined. It is shown that the orientation of the dipolar colloidal particle can efficiently be controlled and changed by locally quenching the nematic liquid crystal from the laser-induced isotropic phase. The interaction of a single colloidal particle with a single colloidal chain is determined and the interactions between pairs of colloidal chains are studied. We demonstrate that dipolar colloidal chains self-assemble into the two-dimensional (2D) dipolar nematic colloidal crystals. An odd-even effect is observed with increasing number of colloidal chains forming the 2D colloidal crystal.

DOI: 10.1103/PhysRevE.76.051406 PACS number(s): 61.30.Jf, 82.70.−y, 47.57.J−

I. INTRODUCTION

Assembling micro- and nanoparticles in regular three-dimensional (3D) geometric patterns is one of the central issues of modern science and technology. A major limitation of self-assembly concepts, which have been developed to date, is the difficulty of scaling them up from the nanoscale to the device dimensions [1–11]. Current concepts rely on particle manipulation using forces of electromagnetic origin (van der Waals, screened electrostatic), which are difficult to control, particularly over macroscopic length scales. For example, scientists have been trying already for a long time to self-assemble 3D photonic crystals from water-based colloidal systems, using sedimentation from colloidal solutions, growth on patterned surfaces, and external assisted manipulation. Despite enormous efforts, the problem of controlled growth of microcolloidal structures from water-based colloidal systems has remained mainly unsolved. It is therefore evident that novel approaches using novel forces and conceptually novel solutions are needed.

A novel approach to self-assembly is to use structural forces in liquid crystals [12–21] to control the spatial arrangement of particles in three dimensions. When particles, such as colloidal microspheres, are introduced into the nematic liquid crystal, the orientation of the nematic molecules is locally disturbed, because of their interaction with surfaces of inclusions. The disturbance spreads on a long (micron) scale and can be considered as an elastic deformation of the nematic liquid crystal. As the elastic energy of deformation depends on the separation between inclusions, structural forces between inclusions are generated.

In contrast to water-based colloidal systems, where the colloidal self-assembly is driven by screened Coulomb, capillary, and van der Waals forces, the forces in nematic colloids offer several advantages: (i) the interparticle interactions in the nematic liquid crystalline media are a thousand times larger compared to the isotropic solvents, (ii) a liquid crystal is an anisotropic solvent, providing spatially anisotropic forces even for simple spherical colloidal inclusions, (iii) structural forces in the nematic liquid crystals are of long range, i.e., ten micrometers, compared to the typical range of several nanometers for screened electromagnetic forces in classic colloids, (iv) the forces in the nematic liquid crystals are hierarchical in nature, implying several characteristic length scales that are susceptible to external electric and magnetic fields. This opens new and exciting routes to nontrivial self-assembly of colloidal particles in anisotropic and complex solvents.

It has been shown that the structural forces between colloidal inclusions in liquid crystals have an amazing diversity of self-assembled or directed self-assembled patterns, such as linear chains of colloidal particles [17,22], regular defect arrays [23], two-dimensional hexagonal and dense colloidal lattices at interfaces [24,25], regular colloidal patterns on freely suspended smectic films [26], particle-stabilized defect gels [27], cellular soft materials [28,29], and 2D colloidal crystals in thin nematic cells [18]. This amazing diversity of structures, which have been discovered in a relatively short period of time, indicates that much more complex colloidal patterns in liquid crystals, featuring new functionalities, could be discovered in the near future in this field.

In this paper we present more detailed experimental and numerical analysis of our recent work on the self-assembly of dipolar colloidal particles in 2D colloidal crystals in thin nematic layers [18]. Experimental procedures and steps, which have led us to the formation of robust 2D dipolar colloidal crystals, are described and explained. We also present analysis of the interactions and stability of different chainlike colloidal structures and describe different phenomena which could be observed in our experiments. The details on related quadrupolar 2D colloidal crystals will be given elsewhere.

II. EXPERIMENT

We have used micron-size silica spheres of diameter $2R=(2.32\pm0.03)$ μm and of the refractive index $n_s=1.37$, which were dispersed in the nematic liquid crystal pentylcyanobiphenyl (5CB). The refractive indices of 5CB are $n_o=1.52$ and $n_e=1.69$ at room temperature. The dielectric anisotropy of 5CB is $\epsilon_a\sim12$ at a temperature of 25 °C. The surface of the silica spheres was first covered with a mono-

layer of N,N-dimethyl-N-octadecyl-3-aminopropyl trimethoxysilyl chloride (DMOAP), which ensures a very strong homeotropic surface anchoring of a nematic liquid crystal. After drying, the colloidal particles were introduced into the liquid crystal at a typical concentration of 0.1%. The nematic colloidal dispersion was then introduced into a thin planar cell with rubbed polyimide alignment layers. The cells were made of two parallel optically transparent indium thin oxide (ITO) coated glasses. ITO coating was used in order to increase the absorption of the laser light and locally melt the nematic in some of the experiments. The planar anchoring on the two boundary glasses was obtained by rubbed polyimide coating. The resulting polyimide surface anchoring is very strong, with a small pretilt angle of only a few degrees. Cells of different thickness were used, with thickness in the range from 2 to 7 μm, as measured by a standard interference technique before filling them with 5CB.

As the surfaces of colloidal particles have been treated chemically to induce perpendicular surface orientation of the nematic, and the surfaces of the confining cell were rubbed unidirectionally to induce parallel orientation, the resulting elastic distortion of the nematic around colloids generated repulsive forces between the colloids and the walls of the cell. The colloidal particles were thus stabilized elastically in the middle of the nematic layer, and the particles in the cell remained mobile for a period of several months. In thinner parts of the wedgelike cells, the colloidal particles were surrounded by a distorted nematic, which had a director field with a symmetry reminiscent of that of an electric quadrupole. In places where the nematic layer was thicker, the colloidal particles were surrounded by a distorted nematic, reminiscent of the symmetry of an electric dipole. We have observed that the transition from the dipolar to quadrupolar structure was clearly visible under the polarizing microscope and occurred at a critical thickness of $h=3.5\mu$m. The structural transition is obviously driven by confinement and the results on this matter will be given elsewhere in the near future. An example of a dipolar colloidal particle is shown in Fig. 1(a), whereas the corresponding structure of the nematic director is shown in Fig. 1(b). The "dipolar" structure can be considered as a pair of two topological point defects: (i) the hyperbolic hedgehog defect [indicated with the letter "A" in Fig. 1(b)], displaced from the surface of the colloidal particle along the rubbing direction, and the radial hedgehog [indicated with "B" in Fig. 1(b)], which can be considered as being located inside the colloidal microsphere. Similar to electric charges in electrostatics, both point defects carry the opposite topological charge of magnitude 1, which reflects the global conservation of topological charges, during the process of inserting the colloidal particles in the homogeneous nematic director field.

We have observed these dipolar colloids spontaneously assembled into chains, with dipoles all aligned in the same direction, as shown in Fig. 1(c). This kind of aggregation is known since the early experiments of Poulin in water emulsions, and has been studied extensively to date. Moreover, we have observed that in some parts of the sample, the colloidal chains form interesting local motives and self-assemble into regions of quasiordered regular 2D structures, as shown in Fig. 1(d). After a careful inspection, one observes interesting features in this figure: (i) in regions labeled "A" and "D" a regular 2D hexagonal colloidal lattice is observed, which seems to be formed by the aggregation of individual colloidal chains; (ii) in regions labeled "B" and "C," an unusual arrangement of colloidal particles is observed. Here the particles are connected with a sort of "nematic bonds," which in some cases connect three colloidal particles with the particle in the center (region labeled "B"), and in other cases connect a plurality of neighboring particles (region labeled "C"). This is a very strong indication that one could build long-range ordered, truly crystalline colloidal structures in two dimensions, under controlled assembly.

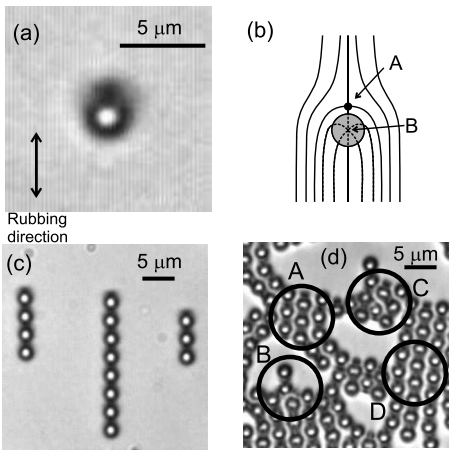

FIG. 1. Dipolar nematic colloids and their aggregation. (a) Unpolarized optical micrograph of a single silica microsphere of dipolar symmetry in 5CB. The hyperbolic hedgehog point defect is visible as a dark spot due to the strong scattering of light. (b) Schematic presentation of the nematic director field around a dipolar colloidal particle. "A" denotes the real hyperbolic hedgehog point defect, "B" denotes the virtual radial hedgehog, located inside the colloidal particle. They form a topological dipole. (c) Dipolar colloidal chains are spontaneously formed in nematic colloids. (d) Spontaneous formation of 2D crystalline colloidal clusters, and various types of "nematic bonds."

In order to assure the controlled assembly, we have systematically studied the directed assembly of dipolar nematic colloids via the following "hierarchy": (i) interaction between two dipolar colloidal particles, (ii) interaction of an isolated dipolar colloidal particle with a dipolar colloidal chain, (iii) interaction between two or many isolated dipolar colloidal chains, and (iv) directed assembly of 2D dipolar colloidal crystals.

We have used laser tweezers to manipulate the colloidal particles in the nematic liquid crystal. The tweezers setup built around an inverted microscope (Zeiss, Axiovert 200 M) with a fast video camera and a cw diode-pumped solid-state laser (Coherent, Compass 2500 MN) at 1064 nm was used as a laser source. An acousto-optic deflector (AOD, IntraAction, model DTD-274HA6), driven by a computerized system (Aresis, Tweez 70) was used for trap manipulation. A beam expander was used to match the laser beam to the AOD aperture and some additional optics was used to image the pivotal point of the AOD onto the entrance pupil of the water immersion microscope objective (Zeiss, IR Achroplan 63/0.9

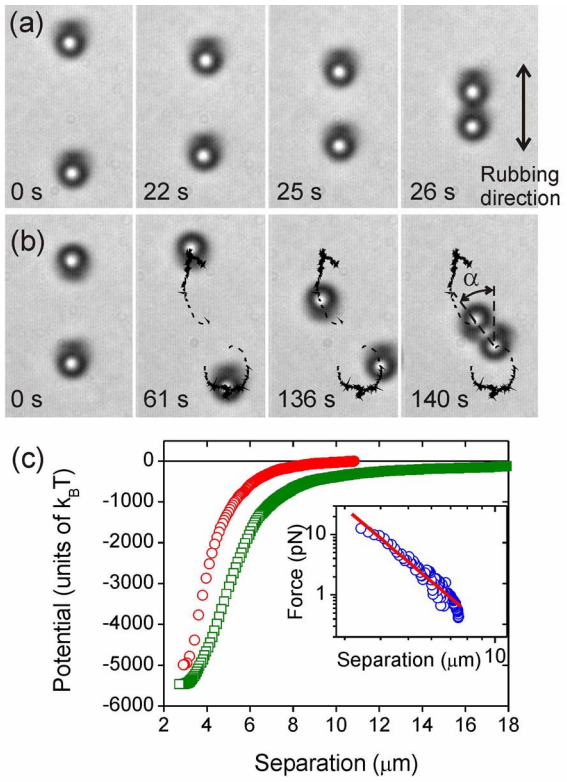

FIG. 2. (Color online) The interaction between two dipolar colloidal particles. (a) Two dipolar colloidal particles with parallel topological dipoles were positioned using the laser tweezers at the initial separation of $\sim 10\mu$m and released. The particles were attracted along the straight line and in the equilibrium position both dipoles were aligned "head to tail." (b) The direction of the upper topological dipole was reversed and the particles were released from the laser traps. Curved trajectories of both particles are clearly revealed, indicating strongly anisotropic attraction. In the equilibrium, both dipoles were antiparallel, with their centers positioned on a line, tilted at $\alpha=36°$ with respect to the rubbing direction. (c) The potential between the two dipolar colloidal particles, as measured along their trajectories, for parallel (circles) and antiparallel (squares) orientation of the two dipoles. The inset shows the dipolar force for parallel orientation and head-to-tail attraction in the log-log plot. The solid line is the $1/r^4$ law.

W). The maximum laser power of a diffraction limited Gaussian beam in the sample plane was up to 50 mW. The laser light was linearly polarized and two orthogonal polarizations could be selected using a rotating half-wave plate.

The forces between two dipolar colloidal particles in the nematic liquid crystal have been studied before [30–35]. Here we briefly describe the pair interaction for colloidal particles with very strong surface anchoring. The sequence of microphotographs in Fig. 2 shows the attraction between the two dipoles in a planar nematic cell with the thickness of $h=6\mu$m for two possible orientations of the dipoles. At the beginning of the experiment, the two colloidal particles were positioned collinearly along the nematic director, with the two dipoles oriented in the same or opposite direction, and released. The corresponding potentials are shown in Fig. 2(c). In both cases, the attraction is of long range and very strong, resulting in the pair binding energy of $\sim 5000k_BT$.

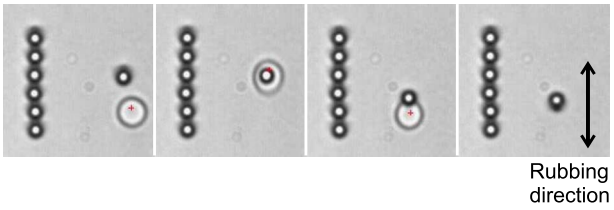

FIG. 3. (Color online) The orientation of the dipolar colloidal particle can be reversed by melting locally the nematic liquid crystal around the particle and "dragging" the molten crystal in a preferred direction for the new orientation of the dipole.

In the next step we have studied the interaction of an isolated dipolar colloidal particle with a dipolar colloidal chain, which was either assembled spontaneously in our sample, or was assembled using the laser tweezers. As there are two stable orientations of a dipolar colloidal particle in a planar nematic cell, a method has been developed to switch the orientation of the dipole from one direction to the opposite. The method is based on locally melting a small area around the selected colloidal particle with laser tweezers and is illustrated in the sequence of images in Fig. 3.

The first image shows a dipolar colloidal particle in the vicinity of the dipolar chain, with the hyperbolic hedgehog defect on top of the single particle. The point defect is visible as a blurred dark spot because of the light scattering. The dark circle below the colloidal particle is a small droplet of the isotropic phase of 5CB, which is separated by a dark interfacial line from the surrounding nematic phase of 5CB. The small cross presents the position of the laser tweezers focus and the applied optical power was 40 mW in a 5-μm-thick planar nematic cell filled with 5CB. The tweezer's focus was positioned on the colloidal particle, so that the isotropic phase symmetrically surrounded the particle. Then, the tweezers was moved "downward" in Fig. 3 at a velocity of $\sim 2\mu$m/s. The third image in this sequence shows the principle of point defect reversal: the colloidal particle is already nearly completely surrounded by the nematic phase. However, it appears as if the hedgehog defect was located inside the isotropic droplet, as it is evidently not located in the rest of the nematic liquid crystal surrounding the particle. Finally, by switching off the light, the isotropic droplet shrank and disappeared, and the hyperbolic hedgehog was created in the position where the isotropic droplet shrank to zero. This is visible in the last image of Fig. 3, where the defect has reappeared on the "bottom" side of the colloidal particle.

Reversal of the dipole orientation with our "melting-dragging" technique can easily be understood. An elastic dipole has a given orientation, as shown in Fig. 3, frame 1. In order to reverse it, we first need to break the orientation, which we do by locally melting the nematic phase around the colloidal particle, as shown in Fig. 3, frame 2. At this stage the director field around the colloidal particle is symmetric with respect to the rubbing direction and therefore the relaxation to possible "up" and "down" dipolar states after switching off the laser is energetically equally favorable. In order to favor one particular dipolar orientation, we need to discriminate these two possibilities, which we do by dragging the

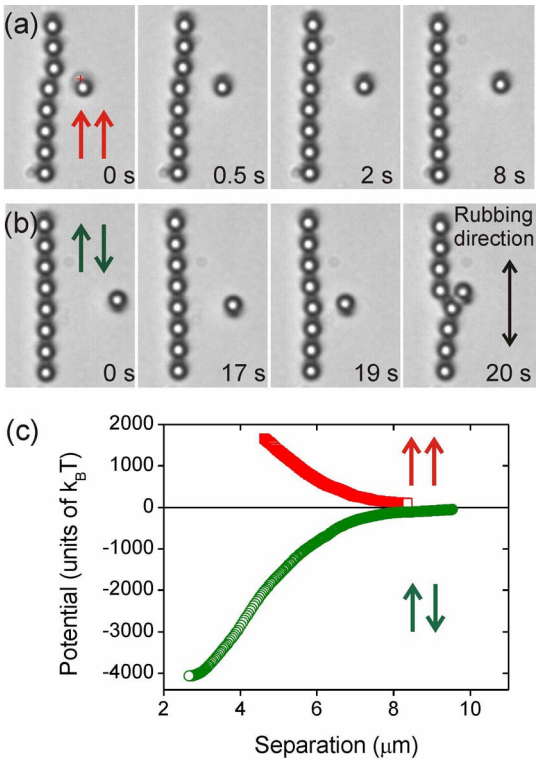

FIG. 4. (Color online) The interaction between a dipolar colloidal chain and an isolated dipolar colloidal particle. The arrows indicate the directions of the topological dipoles. (a) For parallel orientation of the topological dipoles and side position, the colloidal particle is repelled from the chain. (b) If the direction of the topological dipole is reversed, the colloidal particle is strongly attracted to the chain. (c) Using the particle tracking software, the energies of repulsion (squares) and attraction (circles) of a single colloidal particle from the dipolar chain are calculated. Note the energy scale and the strength of interaction.

colloidal particle (Fig. 3, frame 3). The liquid crystal is molten only on the dragging side of the particle and thus, after switching off the laser, the molten region can act as a "source" of the local orientational disorder and the hyperbolic point defect can form on that prechosen side. The method of reversing the direction of the dipolar colloidal particle is therefore simple and proceeds via spatial manipulation of a small isotropic droplet, created by the high-intensity laser tweezers in the nematic layer. The defect always appears on that side of the particle, which is last in contact with the isotropic droplet. This is a very important procedure in the "fabrication" of ordered colloidal nematic structures.

Having control over the orientation of the dipolar colloidal particle, we have investigated the forces between a single dipolar colloidal particle with the predetermined direction of the topological dipole and a dipolar chain. The particles were prepared with preferred orientation of their dipoles and positioned close to the dipolar chain using the laser tweezers. Figure 4(a) shows the interaction of a dipolar colloidal particle with the dipolar chain, where both dipoles point in the same direction. The repulsive force is clearly visible, and the particle is strongly repelled from the chain. The opposite is observed for the antiparallel orientation of the dipoles, as shown in Fig. 4(b): the antiparallel dipolar colloidal particle is strongly attracted and incorporated into the dipolar chain. This observation is extremely important for our further understanding of the stability of 2D dipolar colloidal structures in thin nematic layers.

The strength of the attraction and repulsion between a single dipolar colloidal particle and the dipolar colloidal chain was measured using video microscopy and the particle tracking method. The movement of the particle toward the chain was video monitored at a rate of 25 frames/s. The position of the center of gravity of the particle was determined by video analysis of the captured frames with an accuracy of ±5nm. Having the recorded time dependence of the separation between the particle and the chain, the effective force acting on the particle has been determined following the Stokes law, $f=6\pi R_{eff}\eta\partial r/\partial t$. Here, the product of the effective particle radius and the viscosity $R_{eff}\eta$ has been determined in a separate experiment for the two orthogonal directions of the particle's movement, i.e., parallel and perpendicular to the rubbing direction. As a result we obtain $R_{eff}\eta_{\|}=6.0\times10^{-8}$kg s^{-1} and $R_{eff}\eta_{\perp}=7.5\times10^{-8}$ kg s^{-1}. Finally, by integrating the force f over the separation, we have determined the effective interaction potential between the particle and the chain. The results of the measurements are shown in Fig. 4(c). As expected, the range of the interaction is long, reaching nearly $\sim10\mu$m, and it is strong. It is necessary to deliver $\sim4000k_BT$ of energy to a single 2.3-μm dipolar colloidal particle to unbind it completely from the dipolar chain, made of eight dipolar colloidal particles.

The observation that a single dipolar colloidal particle in the nematic liquid crystal is strongly attracted to a dipolar colloidal chain is an important step toward directed and/or self-assembly of macroscopic 2D dipolar nematic colloidal crystals. Namely, it is easy to understand that following the same reasoning, two dipolar chains with antiparallel dipole moments should attract, whereas chains with parallel dipole moments should repel. This is indeed observed in the experiments. Figure 5(a) shows a strong attraction between two dipolar colloidal chains with antiparallel dipoles, which were separated by $\sim10\mu$m at the beginning of the experiment. In 20 s these two chains were driven into a close contact by the attractive structural force, as evidenced by the last image of the sequence in Fig. 5(a). The drag force on a colloidal chain which is attracted to the neighboring chain is $\vec{f}=\gamma\cdot\vec{v}$. The unknown friction coefficient γ for the colloidal chain was measured in a separate experiment, where the thermal Brownian motion of the chain assembled of five particles was monitored and analyzed. The friction coefficient of such a chain is approximately 4.2 times larger than the friction coefficient of a single colloidal particle. The interaction potential of a chain is calculated by integrating the work of the drag force along the path. It is strong and equals $\sim10.000k_BT$ per chain, assembled of five dipolar particles, as shown in Fig. 5(b).

An interesting odd-even phenomenon is observed with dipolar chain attraction, which is shown in the sequence of images in Fig. 6. When the number of assembled chains is even, they are tilted at an angle β with respect to the rubbing

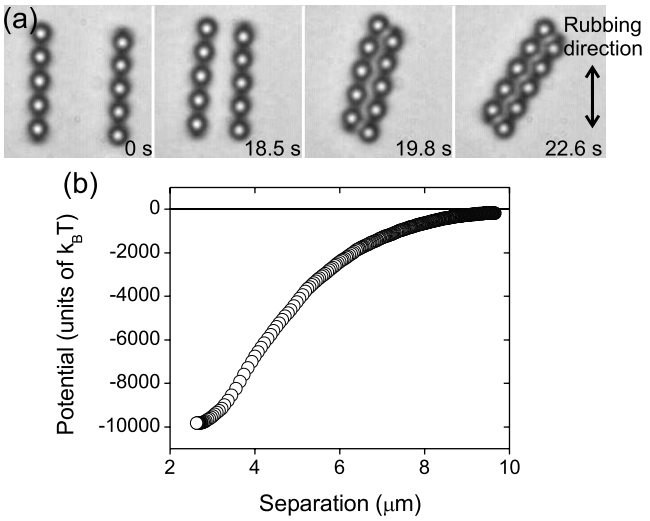

FIG. 5. Attraction between a pair of dipolar nematic colloidal chains. (a) Two dipolar colloidal chains with reversed directions of their topological dipoles were assembled, positioned close to each other, and released. Note the tilting of the assembly, as it approaches the equilibrium position. (b) The interaction energy between a pair of dipolar colloidal chains.

direction. For an odd number of chains, the assembly is oriented along the rubbing direction. A single pair of dipolar colloidal chains, assembled into "2D" nematic colloidal crystal, is tilted at an angle $\beta=33°$ with respect to the rubbing direction. The magnitude of β decreases with increasing number N of the assembled colloidal chains, as shown in Fig. 6(e).

The reason for this odd-even effect is illustrated in Figs. 7(a) and 7(b) and is due to the minimization of the elastic distortion of the nematic liquid crystal. Figure 7(a) illustrates the regions of strong elastic distortion for a pair of dipolar

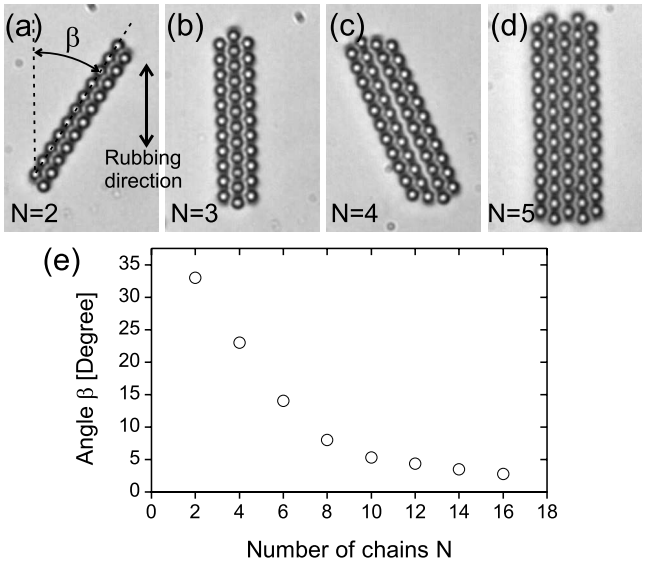

FIG. 6. (a)–(d) Odd-even effect in the tilt of 2D dipolar nematic colloidal assemblies. (e) The tilt angle of the dipolar colloidal assembly as a function of the number of colloidal chains. Even numbers only are shown.

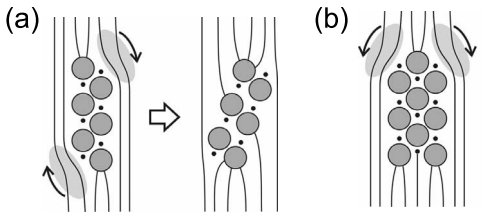

FIG. 7. Origin of the odd-even effect in the tilt of the colloidal chains. (a) For an even number of dipolar nematic colloidal chains, regions of strong elastic deformation are present, when the assembly is oriented along the rubbing direction. This strain can be released by tilting the 2D assembly. (b) The 2D nematic colloidal crystal, composed of an odd number of dipolar colloidal chains, is symmetrically distorted. Any rotation does not decrease the energy of deformation.

colloidal chains in the case when they are oriented along the rubbing direction. It is energetically more favorable to relax this strong elastic distortion by a slight rotation of a crystal as a whole in the clockwise direction. Upon rotation, the regions of strong distortion (shaded areas) are minimized, and the total free energy of the system is decreased. For an odd number of assembled chains, as shown in Fig. 7(b), the distortion appears symmetrically on both sides of the 2D colloidal assembly, and there is no reason for rotation, as this leads to no decrease of the free energy. This explains qualitatively the observed odd-even phenomenon.

Our understanding of how the dipolar colloidal chains assemble into 2D colloidal nematic crystals and knowing how to control the direction of the single topological dipole allows for directed assembly of large scale 2D nematic colloidal crystals. Figure 8(a) presents an example of a laser tweezers-assembled 2D nematic crystal with 280 colloidal particles. The assembly consists of 17 shorter dipolar chains of eight colloidal particles pointing downward with their topological dipoles and 16 longer dipolar colloidal chains of nine colloidal particles pointing upwards with their dipoles. Figure 8(b) presents the basic principle of binding dipolar colloidal chains into 2D colloidal nematic crystals. Each dipolar colloidal chain can be considered as a topologically "ferroelectric" object that attracts an oppositely oriented neighboring ferroelectric topological chain, thus forming a topologically "antiferroelectric" chain assembly. This assembly in turn attracts other ferroelectric chains in the "up-down-up-down..." manner, so that the antiferroelectriclike 2D nematic colloidal crystals of an arbitrary size can be assembled.

The details of the crystalline unit cell are shown in Fig. 8(c), which is a zoom-in of the selected area from Fig. 8(a). The 2D dipolar colloidal nematic crystal has a general parallelogram unit cell with the lattice constants $a=(2.95\pm0.03)$ μm, $b=(2.84\pm0.02)$ μm, and $\gamma=(61\pm1)°$, as indicated in Fig. 8(c). This unit cell corresponds to 520-nm surface-surface separation between the colloidal particles along the chains ($\vec{b}$ direction) and 640-nm separation between the nearest colloidal particles in sequent ferroelectric chains (i.e., $\vec{a}$ direction). The 2D colloidal crystalline structure is extremely robust against external perturbations and remains stable for several months. The crystal could also

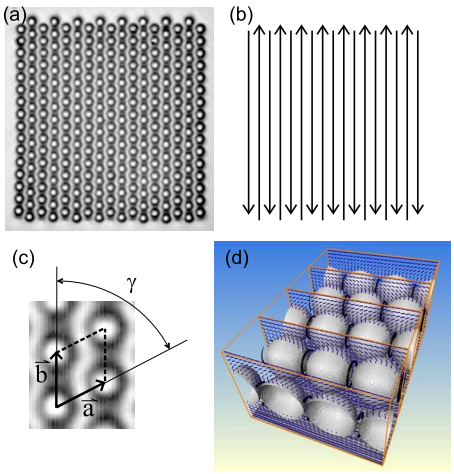

FIG. 8. (Color online) (a) An example of a 2D dipolar nematic colloidal crystal, assembled by the laser tweezer's manipulation. The crystal consists of 280 silica spheres and is stable for more than a year at laboratory conditions. (b) Schematic drawing of the direction of the topological dipoles of each dipolar chain. Each chain can be considered as a "ferroelectric" object, which are packed in the "antiferroelectric," up-down manner, thus filling the 2D space. (c) The lattice vectors and the unit cell of the dipolar colloidal crystal shown in (a). (d) The result of the LdG modeling of the stability of 2D dipolar nematic colloidal crystal in a thin nematic cell. The lines denote the orientation of the director field. Thick dark circles between the colloidal particles are small topological rings that have developed from a hedgehog point defect due to strong confinement.

be grabbed by the laser tweezers and slowly moved to a new position as a single whole, which illustrates its extreme robustness.

III. THEORY

We have examined the stability of a 2D system of colloidal particles, confined to a thin nematic layer using the Landau–de Gennes (LdG) formalism with full tensorial description. Namely, when dealing with small colloidal particles and defects in liquid crystals, the Landau–de Gennes description [36] based on the full nematic order parameter tensor Q_{ij} is most appropriate, as it takes into account not only Frank elasticity due to the deformation of the nematic director field, but also local variations of the degree of order and possible biaxiality. The order parameter tensor is a 3×3 symmetric traceless matrix, whose invariants are used to construct the free energy F of the nematic, constrained by the colloidal particles and the surfaces of the cell:

$$F = +\frac{1}{2}L\int_{LC}\left(\frac{\partial Q_{ij}}{\partial x_k}\right)\left(\frac{\partial Q_{ij}}{\partial x_k}\right)dV + \int_{LC}\left(\frac{1}{2}AQ_{ij}Q_{ji} + \frac{1}{3}BQ_{ij}Q_{jk}Q_{ki} + \frac{1}{4}C(Q_{ij}Q_{ji})^2\right)dV + \frac{1}{2}W\int_{Surf.Col.}(Q_{ij}-Q_{ij}^0)(Q_{ji}-Q_{ji}^0)dS. \quad (1)$$

The first term in Eq. (1) describes the increase of the free energy due to spatial variations of the nematic orientation and order, whereas the second term represents the contribution to the free energy due to the magnitude of the nematic order. The interaction of the nematic with surfaces of the colloidal particles is represented by the third Rapini-Papoular-type term. We have chosen a single elastic constant approximation (L); A, B, and C are the conventional nematic material constants, W is the strength of the surface anchoring, and Q_{ij}^0 is the order parameter preferred by the surface. The average orientation of the nematic molecules is set parallel to the confining surfaces with the bulk value of the order parameter. The free energy therefore covers all three fundamental liquid crystal phenomena relevant to our experiments: elasticity, possible formation of defects, and finite interaction of a liquid crystal with surfaces of the colloids.

To obtain the equilibrium order parameter tensor profile, the free energy F was minimized according to the Euler-Lagrange formalism:

$$\frac{d}{dx_k}\frac{\partial f}{\partial(\partial Q_{ij}/\partial x_k)} - \frac{\partial f}{\partial Q_{ij}} = 0, \quad (2)$$

$$\frac{\partial f}{\partial(\partial Q_{ij}/\partial x_k)}\cdot\nu_k = 0, \quad (3)$$

where f is the free energy volume density introduced as $F=\int f dV$, ν_k is the colloidal surface normal, and summation over repeated indices is assumed. Equation (2) determines bulk behavior of the order parameter tensor, as Eq. (3) describes the surface and acts as a boundary condition on the particle walls. Evaluating Eqs. (2) and (3) for the chosen free energy functional F, one gets for each component of the order parameter tensor Q_{ij} the following governing equations:

$$L\nabla^2 Q_{ij} - AQ_{ij} - BQ_{ik}Q_{kj} - CQ_{ij}(Q_{kl}Q_{lk}) = 0, \quad (4)$$

$$L\frac{\partial Q_{ij}}{\partial x_k}\nu_k + W(Q_{ij}-Q_{ij}^0) = 0. \quad (5)$$

Here, Eq. (4) is the bulk equation and Eq. (5) describes the boundary condition on the colloidal surfaces. Since Q_{ij} is symmetric, a set of only six coupled nonlinear partial differential equations is obtained, with an additional constraint that Q_{ij} has to remain traceless, and needs to be solved.

This system of coupled nonlinear partial differential equations with proper boundary conditions was solved numerically by an explicit Euler finite difference relaxation algorithm on a cubic mesh [37]. In calculations the following numerical parameter values: $L=4.0\times10^{-11}$ N, $A=-0.172\times10^6$ J/m^3, $B=-2.12\times10^6$ J/m^3, $C=1.73\times10^6$ J/m^3, $W=1.0\times10^{-2}$ J/m^2, $R=0.5$ μm, and cell thickness 2 μm, which corresponds the bulk scalar order parameter $S_0=0.533$ and the nematic correlation length $\xi_N=\sqrt{\frac{3L}{3A+3BS_0+27CS_0^2/2}}=6.63$ nm. Further, we have chosen an orthorhombic unit cell with total of 2 ($2=1+4\times1/4$) colloidal particles positioned at the center of the cell. Finally, let us

comment that the constraint of Q_{ij} being traceless was implemented directly into the numerical algorithm, which corrected Q_{ij} after every iterative step.

At these parameter values and geometry several equilibrium order parameter tensor profiles and thus also defect configuration exist as a solution of the Euler-Lagrange equations, depending primarily on the initial conditions of the order parameter tensor profile (more on this will be given elsewhere). To ensure that in our periodic simulation cell indeed antiparallel dipolar chains will form and to speed up the relaxation process, all calculations were started from a prepared initial condition. For the initial condition in the close surroundings of each colloidal particle i, the tensor profile was chosen to have its director component as obtained from a multipole expansion:

$$\vec{n} = \vec{e}_x \pm qR^2 \frac{\vec{r} - \vec{r}_i}{|\vec{r} - \vec{r}_i|^3}, \tag{6}$$

where $\vec{e}_x$ is a unit vector pointing in the director far-field direction, q is a constant which determines the initial position of the point defect (or even small ring)—we have used $q=3.73$, $\vec{r}_i$ is the position of the ith colloid, $\vec{r}$ is a position vector, and by switching plus and minus one can control the orientation of the elastic dipole. Note that this 2D dipolar configuration can be reached also from a completely disoriented initial condition, but within more iteration steps.

The numerical results for a stable 2D nematic colloidal crystal, confined to a thin nematic layer, are shown in Fig. 8(d). Due to the strong confinement and relatively small ratio between the colloidal radius and nematic correlation length ($R/\xi_N=75$), the -1 point defect has opened into a small defect ring with the same topological properties. The effective potential F, which binds together the 2D dipolar colloidal crystal, is very strong and highly anisotropic, showing strong binding in the direction of dipolar chains and relatively weaker binding in the direction perpendicular to the chains. At this point we should also comment that the confinement in our calculations was much stronger compared to the experiment, resulting in much smaller equilibrium separations between the colloidal particles. The calculated lattice constants were $a=1.26d$, $b=1.02d$, and the calculated equilibrium angle of the oblique unit cell was $\gamma=(66\pm1)°$.

The stability of 2D nematic colloidal crystals can be qualitatively understood as a result of two opposing mechanisms. On one hand, the liquid crystal tries to keep the perturbed volume as small as possible, while on the other hand it also strongly dislikes strong deformation, when the colloidal particles are highly confined. A delicate balance between these two effects governs the positional and orientational ordering of the nematic colloidal crystal.

IV. DISCUSSION AND CONCLUSIONS

There are three important aspects of our work on the stability and self-assembly of 2D nematic colloidal crystals. First, we have demonstrated an important conceptual step from 1D to 2D colloidal structures. Similar to the mechanism which is responsible for the stability and assembly of 1D dipolar colloidal chains, the 2D nematic colloidal crystals are bound by sharing the common regions of the elastic deformation and defects between the colloidal particles. There is no doubt that such a concept could by applied to assemble the 3D nematic colloidal structures, which would be a unique achievement in colloidal science in general. A step of spontaneous or directed colloidal assembly from 2D to 3D would open a variety of possible technological applications, such as assembly of 3D photonic crystals for optical processing and sensing.

Second, the 2D nematic colloidal crystals are extremely robust structures, which could be manipulated using laser tweezers or microfluidic devices. A typical colloidal binding energy in the nematic colloidal crystals is of the order of $4000k_BT$ for 2-μm-diameter colloidal particles. As such, it is nearly two to three orders of magnitude larger compared to the water-based colloids, where a typical binding energy is of the order of only several k_BT for the particles of similar sizes. This difference is due to the different nature of the binding forces in both systems. In water-based colloids, the stability of colloidal structures relies on the fine balance between the weak attractive van der Waals and repulsive screened electrostatic repulsion due to the surface charge of colloidal particles. The weakness of these interactions has some advantages with respect to the spontaneous self-assembly, as the colloidal particles can explore during their Brownian motion many possible metastable configurations and settle in the global free energy minimum. Whereas this avoids jamming and freezing of unwanted irregular structures, the resulting self-assembled structures are extremely fragile and not applicable to possible technological processing to produce large scale integrated devices. On the other hand, the nature of colloidal interactions is quite different in nematic solvents. In contrast to relatively short range, screened interactions in water-based colloids, the structural interaction in nematic colloids are of long range and effective over the separation, comparable to the thickness of the confined nematic layer. Namely, the confinement also acts as a screening mechanism in confined nematic colloids, but the dipolar colloidal interactions are still significant over the separations of the order of 10μm. This is a very important aspect for possible technological processing, using sophisticated methods of massive colloidal transport, such as microfluidics or optoelectronic tweezers.

Third, we have found an extremely good agreement between the experiment and theoretical LdG analysis of nematic colloids. This is also a very important aspect, as we are confident that the theory can predict unknown and possibly more complex structures with high accuracy and probability. This can dramatically reduce experimental efforts and could be used for strategic planning in the development of novel nematic colloidal structures of high complexity and novel functionality.

In conclusion, we have shown that a delicate balance of structural forces in the nematic colloids not only leads to new and fascinating self-assembling phenomena, but also opens new and exciting pathways to the self-assembly of complex colloidal systems and presents a novel paradigm in colloidal science.

[1] G. Binnig and H. Rohrer, Helv. Phys. Acta **55**, 726 (1982).
[2] M. P. MacDonald, G. C. Spalding, and K. Dholakia, Nature (London) **426**, 421 (2003).
[3] D. G. Grier, Nature (London) **424**, 810 (2003).
[4] P. Yu Chiou, A. T. Ohta, and Ming C. Wu, Nature (London) **436**, 370 (2005).
[5] D. Psaltis, S. R. Quake, and C. Yang, Nature (London) **442**, 381 (2006).
[6] A. Aoki, H. T. Miyazaki, H. Hirayama, K. Inoshita, T. Baba, K. Sakoda, N. Shinya, and Y. Aoyagi, Nat. Mater. **2**, 117 (2003).
[7] V. W. A. de Villeneuve, R. P. A. Dullens, D. G. A. L. Aarts, E. Groenveld, J. H. Scherff, W. K. Kegel, and H. N. W. Lekkerkerker, Science **309**, 1231 (2005).
[8] J. D. Joannopoulos, P. R. Villeneuve, and S. Fan, Nature (London) **386**, 143 (1997).
[9] A. van Blaaderen, R. Ruel, and P. Wiltzius, Nature (London) **385**, 321 (1997).
[10] Y. A. Vlasov, J. C. Xiang-Zheng Bo, J. C. Sturm, and D. J. Norris, Nature (London) **414**, 289 (2001).
[11] M. E. Leunissen, C. G. Christova, A. P. Hynninen, C. P. Royall, A. I. Campbell, A. Imhof, M. Dijkstra, R. van Roij, and A. van Blaaderen, Nature (London) **437**, 235 (2005).
[12] P. Poulin, V. A. Raghunathan, P. Richetti, and D. Roux, J. Phys. II **4**, 1557 (1994).
[13] S. Ramaswamy, R. Nityananda, V. A. Raghunathan, and J. Prost, Mol. Cryst. Liq. Cryst. **288**, 175 (1996).
[14] V. A. Raghunathan, P. Richetti, D. Roux, F. Nallet, and A. K. Sood, Mol. Cryst. Liq. Cryst. **288**, 181 (1996).
[15] O. V. Kuksenok, R. W. Ruhwandl, S. V. Shiyanovskii, and E. M. Terentjev, Phys. Rev. E **54**, 5198 (1996).
[16] R. W. Ruhwandl and E. M. Terentjev, Phys. Rev. E **55**, 2958 (1997).
[17] P. Poulin, H. Stark, T. C. Lubensky, and D. A. Weitz, Science **275**, 1770 (1997).
[18] I. Muševič, M. Škarabot, U. Tkalec, M. Ravnik, and S. Žumer, Science **313**, 954 (2006).
[19] H. Stark, Phys. Rep. **351**, 387 (2001).
[20] T. C. Lubensky, D. Pettey, N. Currier, and H. Stark, Phys. Rev. E **57**, 610 (1998).
[21] P. G. Petrov and E. M. Terentjev, Langmuir **17**, 2942 (2001).
[22] J. C. Loudet, P. Poulin, and P. Barois, Europhys. Lett. **54**, 175 (2001).
[23] M. Yada, J. Yamamoto, and H. Yokoyama, Langmuir **18**, 7436 (2002).
[24] V. G. Nazarenko, A. B. Nych, and B. I. Lev, Phys. Rev. Lett. **87**, 075504 (2001).
[25] A. B. Nych, U. M. Ognysta, V. M. Pergamenshchik, B. I. Lev, V. G. Nazarenko, I. Muševič, M. Škarabot, and O. D. Lavrentovich, Phys. Rev. Lett. **98**, 057801 (2007).
[26] M. Conradi, P. Ziherl, A. Šarlah, and I. Muševič, Eur. Phys. J. E **20**, 231 (2006).
[27] M. Zapotocky, L. Ramos, P. Poulin, T. C. Lubensky, and D. A. Weitz, Science **283**, 209 (1999).
[28] S. P. Meeker, W. C. K. Poon, J. Crain, and E. M. Terentjev, Phys. Rev. E **61**, R6083 (2000).
[29] J. Anderson, E. M. Terentjev, S. P. Meeker, J. Crain, and W. C. K. Poon, Eur. Phys. J. E **4**, 11 (2001).
[30] P. Poulin, V. Cabuil, and D. A. Weitz, Phys. Rev. Lett. **79**, 4862 (1997).
[31] M. Yada, J. Yamamoto, and H. Yokoyama, Phys. Rev. Lett. **92**, 185501 (2004).
[32] C. M. Noel, G. Bossis, A.-M. Chaze, F. Giulieri, and S. Lacis, Phys. Rev. Lett. **96**, 217801 (2006).
[33] I. I. Smalyukh, O. D. Lavrentovich, A. N. Kuzmin, A. V. Kachynski, and P. N. Prasad, Phys. Rev. Lett. **95**, 157801 (2005).
[34] J. Kotar, M. Vilfan, N. Osterman, D. Babič, M. Čopič, and I. Poberaj, Phys. Rev. Lett. **96**, 207801 (2006).
[35] M. Škarabot, M. Ravnik, D. Babič, N. Osterman, I. Poberaj, S. Žumer, I. Muševič, A. Nych, U. Ognysta, and V. Nazarenko, Phys. Rev. E **73**, 021705 (2006).
[36] P. G. de Gennes and J. Prost, *The Physics of Liquid Crystals*, 2nd ed. (Oxford Science Publications, Oxford, 1993).
[37] W. H. Press, B. P. Flannery, S. A. Teukolsky, and W. T. Vetterling, *Numerical Recipies* (Cambridge University Press, Cambridge, England, 1986).